Removal of Orange II by Phosphonium-modified Algerian Bentonites

S. Bouzid [a] , A. Khenifi [a] , K. A. Bennabou [a] , R. Trujillano [b] , M. A. Vicente [b] & Z. Derriche [a]

[a] Laboratoire de Physico-Chimie des Matériaux, Département de Chimie , Université des Sciences et de la Technologie d'Oran , Oran El Menouer , Algéria

[b] GIR QUESCAT, Departamento de Química Inorgánica , Universidad de Salamanca , Salamanca , Spain

PLEASE SCROLL DOWN FOR ARTICLE

Taylor & Francis
Taylor & Francis Group

Removal of Orange II by Phosphonium-modified Algerian Bentonites

S. BOUZID[1], A. KHENIFI[1], K. A. BENNABOU[1], R. TRUJILLANO[2], M. A. VICENTE[2], and Z. DERRICHE[1]

[1]*Laboratoire de Physico-Chimie des Matériaux, Département de Chimie, Université des Sciences et de la Technologie d'Oran, Oran El Menouer, Algéria*
[2]*GIR QUESCAT, Departamento de Química Inorgánica, Universidad de Salamanca, Salamanca, Spain*

An Algerian montmorillonite was modified with two organic surfactants, methyltriphenyl phosphonium bromide and n-hexyltriphenyl phosphonium bromide. The solids obtained were used as adsorbents to remove Orange II, an anionic dye from aqueous solutions. Batch experiments were conducted to study the effects of temperature (20–60°C), initial concentration of adsorbate (50–150 mg L^{-1}) and pH of solution 6.5 on dye adsorption. Due to their organophilic nature, exchanged montmorillonites were able to adsorb Orange II at a very high level. Adsorption of Orange II for B-NHTPB and B-MTPB at different pH show that the adsorption capacity clearly decreases with an increase in pH of the initial solution from 2 to 8, this decrease being dramatic for pH > 8. This may be due to hydrophobic interactions of the organic dye with both phosphonium molecules and the remaining non-covered portion of siloxane surface. The kinetics of the adsorption was discussed on the basis of three kinetic models, i.e., the pseudo-first-order, the pseudo-second-order, and the intraparticle diffusion models. Equilibrium is reached after 30 min and 60 min for B-MTPB and B-NHTPB, respectively; the pseudo-second-order kinetic model described very well the adsorption of Orange II on modified bentonites. The non-linear Langmuir model provided the best correlation of experimental data, maximum adsorption of Orange II is 53.78 mg g^{-1} for B-NHTPB and 33.79 mg g^{-1} for B-MTPB. The thermodynamic parameters, such as free energy of adsorption ($\Delta G°$), enthalpy change ($\Delta H°$), and entropy change ($\Delta S°$) were also determined and evaluated. From thermodynamic studies, it was deduced that the adsorption was spontaneous and exothermic.

Keywords: Adsorption; Alkyltriphenyl phosphonium bromide; Modified montmorillonite; Orange II dye

Introduction

The textile industry is confronted with serious environmental problems associated with its immense wastewater discharge, substantial pollution load, extremely high salinity, and alkaline, heavily colored effluents (Vogelpohl and Kim, 2004). Industrial dyes usually have complex aromatic molecular structures which make them very stable and difficult to biodegrade. Furthermore, many dyes are toxic to some microorganisms and may cause direct destruction or inhibition of their catalytic capabilities (Santhy and Selvapathy, 2006) Dyeing effluents are very difficult to treat, due to their resistance to biodegradability, and stability to light, heat, and oxidizing agents. In general, the treatment of dye-containing effluents is undertaken by adsorption, oxidation-ozonation, biological processes, and coagulation-flocculation and membrane processes (Walker and Weatherley, 1999).

In contrast, adsorption has been accepted as an effective and economical technology to concentrate and remove contaminants from aqueous phases and soils. Most commercial systems currently use activated carbon as a sorbent to remove dyes in wastewater because of its excellent adsorption ability. But it has the disadvantage of the high costs associated with its replacement and regeneration. This limitation has encouraged the search for inexpensive and readily available adsorbents like natural and waste materials. Studies with clays, chitin, algae, agricultural waste residues, fly ash, hydroxide metal sludge, and sewage sludge have been found in the literature (Sílvia et al., 2008). Bentonites are argillaceous materials that can be effectively employed as adsorbents for many wastewater pollutants due to their high specific surface area. This outstanding capability is due to the presence of the mineral montmorillonite. The use of bentonite in wastewater treatment has received increasing attention and currently offers a very attractive method for pollution remediation. Besides it is plentiful, inexpensive, and available in many countries (Khenifi et al., 2007). Bentonite is the most widely studied clay used to prepare organo-clays for decolorizing dye waste water (Baskaralingam et al. 2006; Özcan et al., 2004).

Organo-clays have attracted substantial attention both in fundamental research and industrial applications because

---

Address correspondence to Z. Derriche, Laboratoire de Physico-Chimie des Matériaux, Département de Chimie, Université des Sciences et de la Technologie d'Oran, BP 1505, Oran El Menouer, Algéria. E-mail: derriche_zoubir@yahoo.com

Color versions of one or more of the figures in the article can be found online at www.tandfonline.com/gcec.

of their high sorptive properties (Lee and Lee, 2004). Intercalation of alkylammonium or alkylphosphonium cations into the clay minerals goes via ion exchange resulting in occupation of an interlayer space of the clay structure. Ion exchange of primary, secondary, tertiary, and quaternary alkylammonium or alkylphosphonium cations changes the hydrophilic surfaces of the clay structure into organophilic, which enables sorption or intercalation of the organic compounds (Hedley et al., 2007; Patel et al., 2007) For example, quaternary ammonium salts have been used very often to turn bentonite into a hydrophobic form (Yilmaz and Yapar, 2004) and recently quaternary phosphonium salts were reported (Hedley et al., 2007). As a result, the modified bentonite adsorption capacity increased dramatically in comparison with natural bentonite. Bentonite and montmorillonite modified with cetylpyridinium (Lee et al., 2001; Zhu and Ma, 2008) and hexadecyl trimethylammonium (HDTMA) (Bae et al., 2000) could both effectively adsorb Orange II from aqueous solutions. The bentonites modified with phosphonium salts have an appreciably higher thermal stability than the ammonium salts-modified bentonites and may be potentially useful materials for melt processing of polymer/layered silicates nanocomposites (Khalaf et al., 1997).

In the present article, we report on the preparation and characterization of phosphonium montmorillonite by the interaction of quaternary phosphonium salts with montmorillonite-rich bentonite clay from Algeria, with the objective of preparing organoclays with high thermal stability. Toward this end, two quaternary phosphonium salts were selected—methyltriphenyl phosphonium bromide (MTPB) and n-hexyltriphenyl phosphonium bromide (NHTPB). The prepared solids were applied to the adsorption of Orange II azo-dye. The goal of this study was to demonstrate the potential of phosphonium exchanged bentonite for removing anionic dye from aqueous solutions, determining the adsorption capacity and the mechanism of the process.

Experimental

Starting Materials

The bentonite used in this work comes from a quarry located in Maghnia (in western Algeria), and was supplied by the Algerian mining company ENOF. It is mainly composed of montmorillonite, and the main impurities are quartz, cristobalite, and calcite. The clay was purified as reported previously and named B-Na (Bouberka et al., 2005). The chemical composition of the purified clay was: 54.90% SiO_2, 1.85% MgO, 27.71% Al_2O_3, 0.08% K_2O, 0.08% CaO, 2.82% Fe_2O_3, 3.14% Na_2O, and 9.4% loss on ignition.

The cation exchange capacity (CEC) was determined by two methods—adsorption of methylene blue and conductimetry. The adsorption of methylene blue was used to determine both the CEC and the total surface area of the material (Bouberka et al., 2005). The conductimetric method was based on the cationic exchange between Mg^{2+} and Ba^{2+}, by titration of Ba-saturated montmorillonite suspension (1 g/100 mL) with a 0.02 M $MgSO_4$ solution (Chiu et al., 1990). The initial surface (S total) of clay evaluated by the

methylene blue method is about 792 m^2/g with a CEC of 101.25 meq./100 g of clay, in agreement with the conductimetric method (CEC = 99 meq./100 g of clay). This surface expressed in m^2/g is calculated according to:

$$SSA = (m(MB)/319.9 \times N \times AMB \times (1/A) \qquad (1)$$

where:

m(MB) = mass of adsorbed methylene blue at the point of complete cation replacement (end point),

N = Avogadro's Number = 6.02×10^{23}/mol,

AMB = area covered by one methylene blue molecule, typically assumed to be 130 $\mathring{A}^2$, according to Hang and Brindley (1970).

Preparation of Organoclays

Two phosphonium surfactants were used to modify the bentonite, namely methyltriphenyl phosphonium bromide, $CH_3(C_6H_5)_3PBr$ (98%), abbreviated MTPB, and n-hexyltriphenyl phosphonium bromide, $CH_3(CH_2)_5(C_6H_5)_3PBr$ (99%), abbreviated NHTPB. These products were provided by Aldrich Chemicals, Germany.

The organo-clays were prepared by exchanging the inorganic cation of bentonite with the phosphonium salts, using the amounts of the phosphonium salts that correspond to 100% of the clay's CEC according to the procedure described elsewhere (Khenifi et al., 2009). To this end, 3 g of B-Na dispersed in 300 mL of hot water was added to the phosphonium suspension under continuous stirring. The resulting suspension was heated overnight at 80°C (Avalos et al., 2008) filtered, and washed several times with hot water until complete elimination of bromide anions (Ag^+ test). Prior to its characterization, the organophilic bentonite is dried in an oven at 60°C. These samples are designated B-MTPB and B-NHTPB, respectively.

Characterization Methods

Powder X-ray diffraction patterns (XRD) of the solids were recorded in the 2θ range of 2–65° by a Siemens D-500 diffractometer (Germany), working at 40 kV and 30 mA, and using filtered Cu Kα radiation ($\lambda = 1.5418 \mathring{A}$). Infrared absorption (FT-IR) spectra were determined on KBr discs between 4000 and 400 cm^{-1} by a Perkin-Elmer 1730 FT-IR spectrometer (USA).

Scanning electron microscopy (SEM) was performed on ground samples using a Digital Scanning Microscope DSM 940 Zeiss (Germany). The sample was coated with a thin gold layer (about 20 nm) by metallization using a Bio-Rad ES100 SEN coating system (Bio-Rad laboratories, Inc., USA).

The zero surface charge characteristics of samples were determined, and using the solid addition (Reyad et al., 2007), 40 mL of 0.1 M KNO_3 solution was transferred to a series of 100-mL stoppered conical flasks. The pH_i values of the solutions were roughly adjusted between 2 and 8 by adding either 0.1 N HCl or NaOH and were measured by using a pH meter. The total volume of the solution in the flask was adjusted exactly to 25 mL by adding KNO_3 solution

of the same strength. The pH$_i$ of the solutions was then accurately noted. Samples of 50 mg were added to each flask, and each flask was securely capped immediately. The suspensions were then kept shaking for 24 hr. The final pH values of the supernatant liquid were noted. The difference between the initial and final Ph (pH$_f$) values (ΔpH) was plotted against the pH$_i$. The point of intersection of the resulting curve with abscissa, at which pH$_0$, gave the pH$_{pzc}$ (Somasekhara et al., 2012).

Adsorption Procedures

Adsorption experiments were conducted in a batch mode because of its simplicity. An aqueous OII solution (Aldrich >85%). with a concentration of 500 mg/L was prepared as stock solution, being used for preparing the rest of the solutions by dilution (Chiang et al. 2009).

The effect of pH was analyzed for a fixed dye concentration (25 mg/L), an organo-bentonite mass of 20 mg, and a total solution volume of 20 mL. The pH of the solution was adjusted to the desired values by using solutions of HCl or NaOH (0.1 M). Generally, each experiment was performed at least twice under the same conditions.

The kinetic study was carried out by adding quantities of 250 mg of organo-bentonite into 250 mL of dye solutions with different concentrations (50, 100, and 150 mg/L). The mixtures were put under constant agitation. The effect of the temperature on the kinetic experiments was studied for a constant dye concentration (150 mg/L), an organo-bentonite mass of 250 mg, and a total volume of 250 mL. The control of the temperature was carried out by a thermostatic bath regulated at temperatures from 20 to 60°C. The adsorption isotherms were carried out for concentrations of dye varying between 30 and 200 mg/L, a constant organo-bentonite mass of 250 mg, a solution volume of 250 mL, and an agitation time of 3 hr at the temperatures of 20, 40, and 60°C to achieve equilibrium.

Once the experiments were finished, the organo-bentonite was separated from the liquid phase by centrifugation at 5000 rpm. The concentration of the supernatant was measured by a colorimeter at $\lambda_{max} = 485$ nm (Chen et al., 2011). The quantity of dye adsorbed by the clay was calculated by the equation:

$$q_e = (C_i - C_e)\frac{V}{m} \qquad (2)$$

where C_i and C_e are the initial and final dye concentrations (mg/L), respectively, m is the mass of adsorbent (g), and V is the solution volume (L). Blank experiments, without dye, were carried out in each series of experiments. Each experiment was repeated at least two times. The typical experimental error is lower than 6% for all the experimental results.

Results and Discussion

Characterization of Bentonites

The X-ray diffraction patterns of treated bentonites clearly indicate that the organophilization process was successful (Figure 1). Natural bentonite shows a basal spacing of 11.93 Å, consistent with montmorillonite containing a
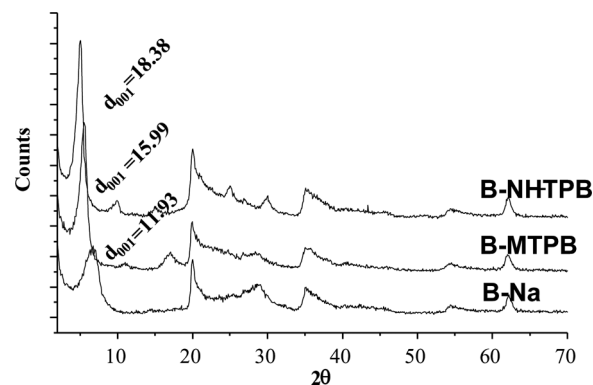

Fig. 1. XRD diffractograms of montmorillonite and organo-montmorillonites.

monolayer of water in the interlayer spacing, which increases to 15.99 and 18.38 Å, for B-MTPB and B-NHTPB, respectively, due to the intercalation of the surfactants into the interlayer of montmorillonite. The value of 15.99 Å for B-MTPB is consistent with a monolayer arrangement of the quaternary phosphonium ions in the interlayer space. The basal spacing of 18.38 Å for the B-NHTPB sample is consistent with a bi-layer arrangement of NHTPB in the interlayer region, as reported by Hedley et al. (2007) for the intercalation of the similar cation butyltriphenylphosphonium (BTPP). This difference in the basal spacing seems to be related to the size of methyl and hexyl groups, the only difference between both phosphonium cations, the larger basal spacing being found for the cation containing the hexyl group. In this sense, Hedley et al. (2007) have reported a basal spacing of 17.7 Å when intercalating butyltriphenylphosphonium (BTPP) into montmorillonite, a value that is consistent with that now found for the sample intercalated with hexyltriphenylphosphonium.

FTIR has been widely used to probe the conformation of the adsorbed surfactant cations on clay minerals. The CH infrared absorption bands are sensitive to the ordering and packing density of the surfactants, and interactions between the alkyl chains (Besson et al., 1987). The FTIR spectrum of the original bentonite is typical of montmorillonite (Figure 2), and logically its bands are maintained in the treated solids, i.e., the bands at 3620 and 3698 cm^{-1} (–OH stretching mode of Al–OH and Si–OH), the broad band centered near 3400 cm^{-1} (stretching mode of water, whose bending mode appears at 1640 cm^{-1}), the peak at 1115 cm^{-1} (out-of-plane Si–O stretching), the band at 1035 cm^{-1} (in-plane Si–O stretching mode), and vibrations at 915, 875, and 836 cm^{-1}, attributed to AlAlOH, AlFeOH, and AlMgOH bending modes (Madejova, 2003). The organophilized solids show in addition the peaks characteristic of the organic molecules, confirming the success of the treatment. Thus, peaks at 1466 cm^{-1} (stretching of aliphatic C–C bonds in a long chain) appeared for B-NHTPB, and a peak at 1379 cm^{-1} (characteristic of methyl groups), and bands at 2850–2855 and 2920–2930 cm^{-1} (asymmetric and symmetric vibrations of C–H, respectively) (Lee and Lee, 2004) appeared in the B-MTPB and B-NHTPB infrared spectra. The main
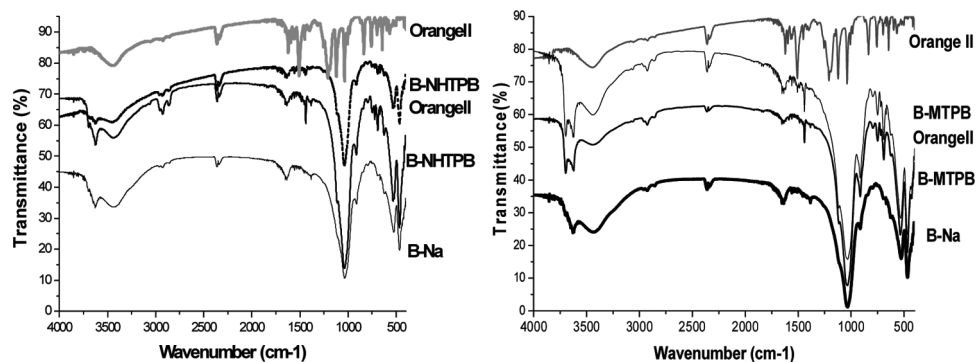
Fig. 2. FTIR spectra of montmorillonite and organo-montmorillonites.

peaks of the aromatic ring at 1436 and 1439 cm^{-1} (bending and stretching of C–C bonds, respectively), 1485, 1511, and 1600 cm^{-1} (stretching vibrations of aromatic C–C bonds), and 2925–3030 cm^{-1} (stretching of C–H aromatic bonds) were also present in both organo-montmorillonites. The phenyl ring attached to the phosphonium atom displayed an unusually sharp and relatively strong vibration band at 1435 cm^{-1} (Patel et al., 2007).

SEM is one of the useful tools to characterize the surface structure of the adsorbent materials. Typical SEM micrographs of adsorbent material were taken before and after dye adsorption and are presented in Figure 3. These micrographs indicated clearly the appearance of the molecular cloud over the surface of phosphonium-loaded clay, which was absent on the rough structure of the clay before loading with phosphonium.

The thermal gravimetric analyses of sodium bentonite (B-Na) and phosphonium organo-montmorillonites (B-MTPB and B-NHTPB) were performed to investigate the effects of phosphonium salts used on the thermal stability of bentonite and the resulting nanocomposites. The mass-loss and derivative mass-loss curves for the natural bentonite are plotted in (Figure 4a); below 200°C, the evolution of

absorbed water and gaseous species, such as physiabsorbed CO_2 and N_2, occurs. Between 250°C and 500°C, organic substances evolve. Dehydroxylation of the aluminosilicate occurs from 500°C to 700°C (Xie et al., 2002). In the case of the organo-bentonite, the first maximum peak of the derivative mass-loss curve took place at a temperature near 70°C. Again, this peak was due to the free water in the organo-bentonite. The weight percentages of free water in the bentonite and organo-bentonite were 12 and 5%, respectively. Thus, the free water diminished when the bentonite was modified with the phosphonium surfactant. This result revealed that the hydrophilic nature of the bentonite was modified with the surfactant and the organo-bentonite surface was organophilic and less hydrophilic.

In contrast, the derivative TGA indicated that the thermal decomposition of the phosphonium surfactants occurred in two steps. In discussing the thermal characteristics of some phosphonium-modified montmorillonites, Xie et al. (2002) have separated the curves into four distinct regions:

1. evolution of free water and gases below 150°C;
2. evolution of organic substances between 150 and 550°C;
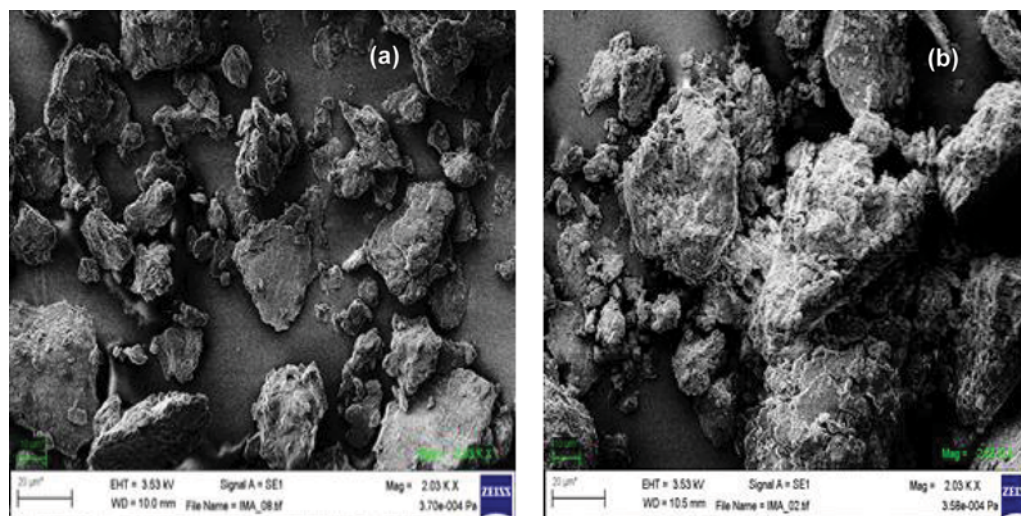3. dehydroxylation of the montmorillonite between 550 and 700°C; and

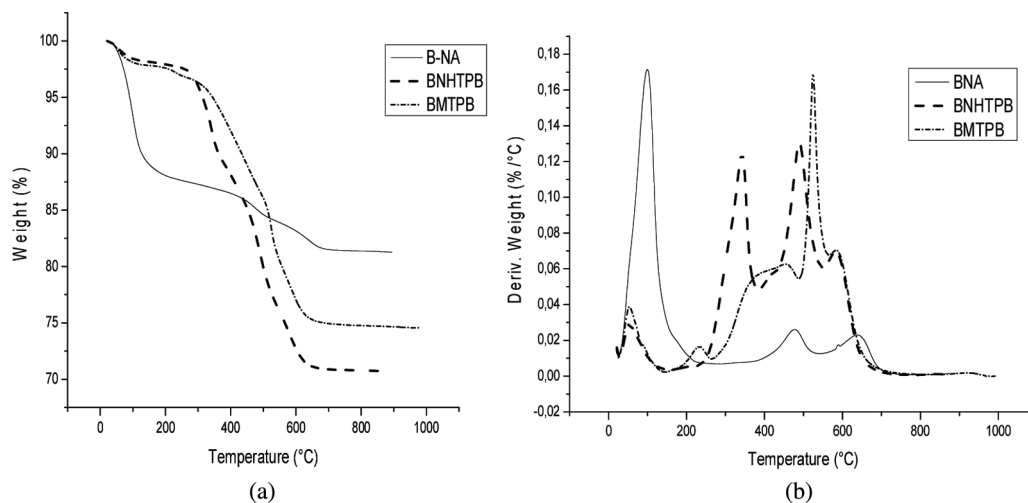**Fig. 3.** Scanning electron microscopy: (a) BNa, (b) B-NHTPB.

Fig. 4. a) Thermogravimetric analysis of purified bentonite, and phosphonium organo-montmorillonites, (b) differential thermogravimetric analysis of purified bentonite, and phosphonium organo-montmorillonites.

4. evolution of carbonaceous residues between 700 and 1000°C.

The DTGA curves in this region (150–500°C) are characterized by a series of exothermic peaks (Figure 4b). Following Xie et al. (2002), the temperature at the onset of the first (prominent) exotherm is taken to represent the point at which the intercalated surfactant begins to decompose. Concerning the phosphonium products patterns, the very large amount of weight loss (35%) was shown at the temperature range of 300–600°C, which is related to the thermal decomposition of the product. The phosphonium salts showed enhanced thermal stability. Thus, in the case of BNHTPB and B-MTPB, the onset temperature of decomposition is close to 350 and 400°C, respectively (Makhoukhi et al., 2008).

Adsorption of Orange II on to B-MTPB and B-NHTPB

Point Charge Zero PZC

The difference between the initial and final pH (pH$_f$) values (ΔpH) was plotted against the pH$_i$. The point of intersection of the resulting curve with abscissa, at which pH$_0$, gave the pH$_{pzc}$. At this pH value a change in surface charge from positive to negative or vice versa occurs (Ijagbemi et al., 2009). The intersection obtained at a pH value of 4 ± 0.1 (data not shown) corresponds to the point of zero charge of the MMT smectite powder.

The surface of the organo-bentonite was charged when the organo-bentonite was placed in a water solution. The surface charge was caused by the interactions between the ions in the solution and the functional groups of the organo-bentonite surface. Normally the surface charge of a solid is dependent on the type of ions present in the solution, the characteristics of the surface, the nature of the adsorbent, and the solution pH. The surface is positively charged when the solution pH is below the PZC, negatively charged at pH above the PZC, and neutral when the pH is equal to the PZC. The PZC of bentonite and montmorillonite has been determined

by several authors (Ijagbemi et al., 2009; Roberto et al., 2008) and is usually acidic in the range 2.3–2.6.

Figure 5 also shows that the Orange II amount adsorbed was found to decrease with an increase in solution pH for the BMTPB. This is because at acidic pH the total surface of the organo-clays (pH$_{PZC}$ 4.6) has more positively charged sites. This does not favor any repulsion between the adsorbent surface and adsorbate. However, at basic pH the ionized species of Orange II were higher than the unionized species (it was found to increase with pH), the Orange II uptake was lower due to the electrostatic repulsions between the negative surface charge (pH$_{pzc}$ < pH (solution)) and the Orange II anions. Similar results were reported in the adsorption of 2, 4, 5-trichlorophenol by organo-montmorillonites (Zaghouane-Boudiaf and Boutahala, 2011).

Effect of pH

The pH is a noteworthy parameter as it has a major effect on the protonation and deprotonation of the adsorbent and adsorbate functional groups, conditioning their electrostatic interaction (Hameed, 2009). Figure 5 shows the adsorption of Orange II for B-NHTPB and B-MTPB at different pH expressed as a percentage of the adsorbate that is actually adsorbed. The adsorption capacity of B-MTPB clearly
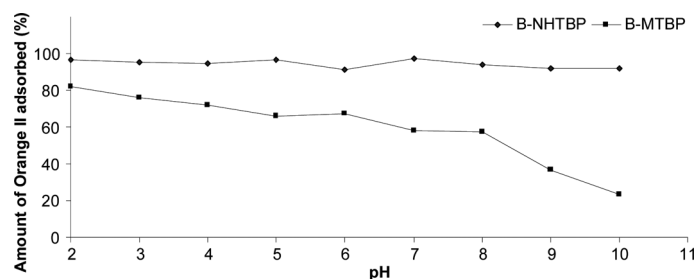

Fig. 5. Effect of pH on adsorption of Orange II by B-MTPB and B-NHTPB, initial dye concentration = 25 mg/L; contact time = 2 h; m/V = 1 g/L.

decreases with an increase in pH of the initial solution from 2 to 10, this decrease being dramatic for pH > 8. The adsorption of anionic dye by phosphonium-modified benonite was attributed to increases in the organophilic character of bentonite due to the intercalation of the surfactants into the interlayer of montmorillonite. Here, hydrophobic interactions of the organic dye should be involved with both phosphonium molecules and the remaining non-covered portion of siloxane surface (Schoonheydt and Johnston, 2006). pH played a key role, more particularly in anionic dye retention (Özcan et al., 2004). Decreasing pH induced an increase of the amount of dye adsorbed on organophilic bentonite, which showed the highest effectiveness (Figure 5).

Besides dye-phosphonium and dye-siloxane surface interactions, acidic media should also promote anion exchange on positively charged $M_t - OH_2^+$ edge sites (Schoonheydt and Johnston, 2006), the density of which is expected to increase with decreasing pH (Lagaly, 2006). Unless low pHs alter the clay mineral structure (Assaad et al., 2007; Permien and Lagaly, 1995), partial dealumination might even be advantageous by providing additional positively charged adsorption edge sites. Figure 3 clearly shows this behavior, and it can be observed that the adsorption capacity of B-MTPB clearly decreases with an increase in pH of the initial solution from 2 to 8, this decrease being dramatic for pH > 8 (Qian et al., 2010; Vinka et al., 2006). Indeed, the molecule of Orange II has two pKa values. The first pKa_1 is at 1.1 and the second pKa_2 at 11.0 (Bandara et al., 1999; Zhiyong et al., 2007). At pH 10, the Orange II molecule is negatively charged and should be electrostatically repulsed by the remaining non-covered portion of siloxane surface of bentonite.

A similar behavior may be expected for B-NHTPB, but the adsorption of Orange II is practically not sensitive to variation of pH. The difference between the two molecules is probably due to the greater extent of hydrophobicity exhibited by B-NHTPB in comparison with B-MTPB, due to the largest hexyl chain compared to methyl (Binoy et al., 2011).

Effect of Contact Time
A brief study of the kinetics of the adsorption was carried out to determine the contact time at which the equilibrium is reached. Figure 6 shows the evolution with time of the amount of OII adsorbed by organo-montmorillonites

at three initial solute concentrations (50, 100, 150 mg/L), while the sorbent dosage and pH were constant (1 g/L and 6.5, respectively).

Generally, the removal of dye was dependent on its initial concentration. The amount of dye adsorbed initially increased when increasing the dye concentration, and remained constant after equilibrium time. Equilibrium is reached after 1 hr of contact. The concentration provides an important driving force to overcome all mass transfer resistance of the dye between the aqueous and solid phases (Ren et al., 2010). The sorption capacity at equilibrium increases from 43.04 to 53.00 mg/g for B-NHTPB, and from 20.25 to 35.51 mg/g for B-MTPB, when the initial dye concentration increased from 50 to 150 mg/L.

The kinetic curves show that the equilibrium time and adsorption capacity of B-NHTPB and B-MTPB are quite different. Using B-NHTPB as adsorbent, the adsorption of OII shows a faster initial step (30 min) and after that it increases slowly until approximately 60 min. For B-MTPB, only 30 min were necessary for reaching equilibrium but the maximum amount of adsorbed Orange II was less than that observed for the first material. This can be related to the larger basal spacing of B-NHTPB, as mentioned previously.

Kinetic Modelling
The adsorption kinetic was modelled as pseudo-first-order, pseudo-second-order, and intra-particle diffusion process (Ho and McKay, 1999).

A pseudo-first-order kinetic equation was used to test the experimental data to examine the controlling mechanism of adsorption processes. This model was proposed by Lagergren for the adsorption in solid/liquid systems and its linear form can be formulated as:

$$\log(q_e - q_t) = \log q_e - \frac{k_1}{2.303}t \qquad (3)$$

where q_t is the adsorption capacity (mg/g) at time t and k_1 (min^{-1}) is the rate constant of the pseudo-first-order adsorption. The k_1 and regression coefficient were calculated from the linear plot of $log(q_e - q_t)$ versus t (Figure 7). The parameters of the pseudo-first-order model are summarized in Table I.

Ho and McKay (1999) developed a pseudo-second-order kinetic expression for the sorption system of dye onto fly
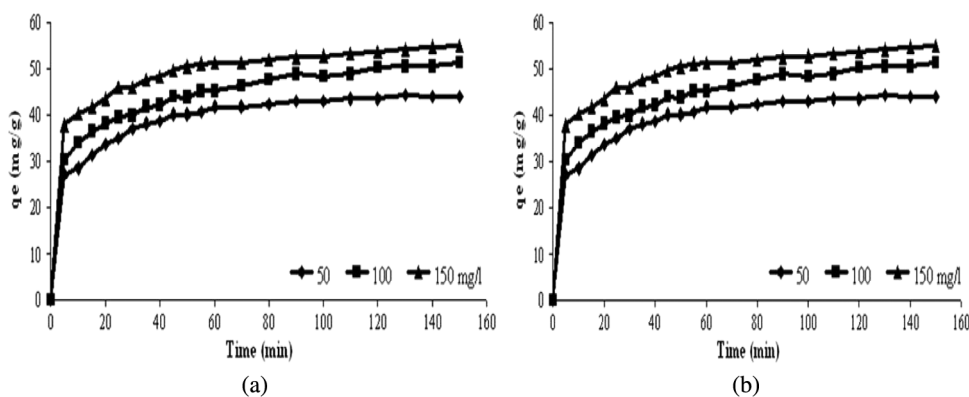

(a)   (b)

Fig. 6. Effect of initial Orange II concentration on the adsorption kinetics of (a) B-NHTPB)-(b) B-MTPB, m/V = 1 g/L, pH = 6.5.
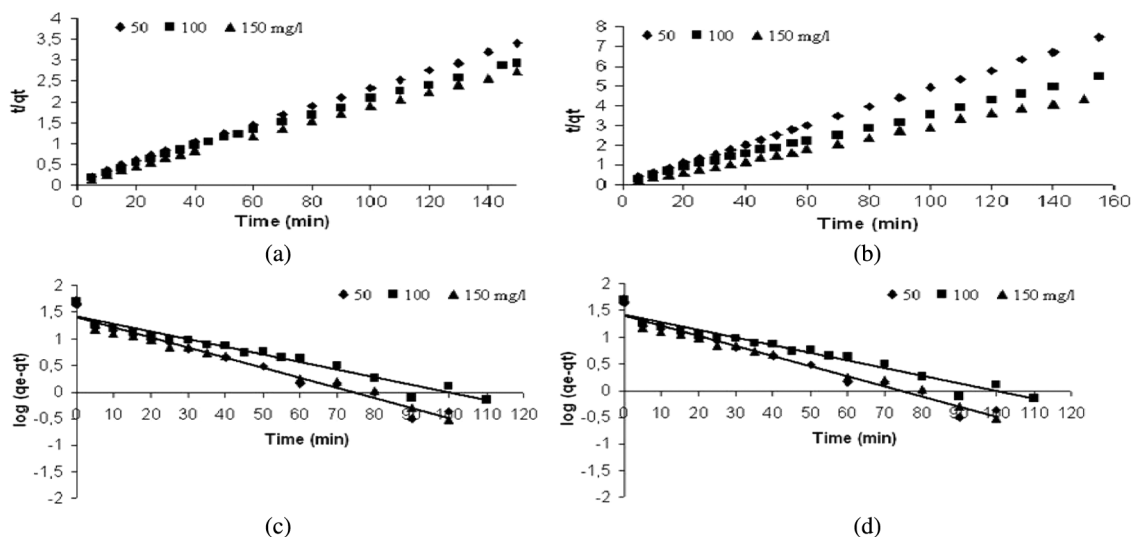
Fig. 7. Pseudo-second-order kinetics for adsorption of Orange II on (a) B- NHTPB and (b) B-MTPB. At various concentrations and, pseudo-first-order kinetics for adsorption of Orange II on (c) B-NHTPB, (d) B-MTPB (m/V, 1 g/ L; pH 6.5, T = 20°C).

ash. This model has been widely applied to a number of dye/adsorbent systems (Aydin et al., 2004). This pseudo-second-order kinetic can be expressed in a linear form as:

$$\frac{t}{q_t} = \left(\frac{1}{K_2 q_e^2}\right) + \left(\frac{1}{q_e}\right)t \qquad (4)$$

where q_e is the amount of OII adsorbed at equilibrium (mg/g), q_t the amount of OII adsorbed at time t(mg/g), and K_2 (g/mg min) is the rate constant of the pseudo-second-order sorption. The values of K_2 are obtained from the slope of the linear plot of t/qt versus t.

The experimental value of solid phase concentration of adsorbate at equilibrium (qe_{exp}) and the calculated values of solid phase concentration of adsorbate at equilibrium for the pseudo-first-order and pseudo-second-order models are shown in Table I. The adsorption first-order rate constants were found to be 0.0414, 0.0310, and 0.0398 min^{-1} for B-NHTPB and 0.0688, 0.0382, and 0.115 min^{-1} for B-MTPB, for concentrations of 50, 100, and 150 mg/L, respectively. The variation in the rate should be proportional to the first power of concentration for strict surface adsorption. However, the relationship between initial solute concentration and rate of adsorption will not be linear when pore diffusion limits the adsorption process (Mohamed et al.,

2012). Figure 7 indicates that the Lagergren model fits well for the first 60 min for B-NHTPB and 30 min for B-MTPB, and thereafter the data deviate from theory. Thus, the model represents the initial stages when rapid adsorption occurs but cannot be applied for the entire adsorption process, a trend previously observed by Ho and McKay (1999).

The qe_{exp} and the q_e values from the pseudo-second-order kinetic model are very close to each other, and the correlation coefficients are closer to unity for pseudo-second-order kinetics than that for the pseudo-first-order kinetics. Therefore, the adsorption of Orange II by B-NHTPB and B-MTPB can be more appropriately correlated by the pseudo-second-order kinetic model. Similar results have been reported for removal of Brilliant Green (BG) by clay adsorbents (Nandi et al., 2009). This suggests that the pseudo-second-order model—based on the assumption that the rate-limiting step may be chemical sorption involving valence forces through sharing or exchange electrons between adsorbent and adsorbate—provides the best description for this process (Ho et al., 1994).

The initial sorption rate can be obtained as qt/t approaches to zero:

$$h = Kq_e^2 \qquad (5)$$

Table I. Kinetics constants for removal of Orange II by B-NHTPB and B-MTPB at different concentrations (V = 250 mL; m = 250 mg; pH = 6.5)

Adsorbent	C_0 (mg/L)	qe_{exp}(mg/g)	q_e(mg/g)	K_1(min^{-1})	R_1^2	q_{2cal} (mg/g)	K_2(g/mg/min)	h (mg/g/min)	R_2^2
B-NHTPB	50	43.04	22.00	0.0414	0.97	45.87	0.0032	6.732	0.99
	100	49.40	22.85	0.0310	0.96	53.47	0.0019	8.432	0.99
	150	53.00	20.89	0.0398	0.98	56.17	0.0032	10.096	0.99
B-MTPB	50	20.25	07.74	0.0688	0.91	21.18	0.0149	6.6840	0.99
	100	26.29	06.91	0.0382	0.88	26.29	0.0120	8.2939	0.99
	150	33.51	08.99	0.115	0.78	34.24	0.0190	22.275	0.99

h increases when increasing the initial dye concentration (Table I), which could be attributed to the increase in the driving force for mass transfer, allowing more dye molecules to reach the surface of the adsorbents in a shorter period of time (Ho and McKay, 1998). Similar phenomena have been observed in the adsorption of anionic dyes on other natural adsorbents modified by surfactants (Sureshkumar and Namasivayam, 2008).

The linearity of the plots of the pseudo-second-order model in Figure 7 indicates that chemical reaction rather than physic-sorption is the main rate-controlling step throughout most of the adsorption process (Vadivelan and Kumar, 2005) and that the mechanism follows a pseudo-second-order reaction scheme.

For the interpretation of experimental kinetics data from a mechanistic viewpoint, prediction of the rate-limiting step is an important consideration. The overall adsorption process may be controlled either by one or more steps—e.g., film or external diffusion, pore diffusion, surface diffusion, and adsorption on the pore surface—or a combination of more than one step (Lakshmi et al., 2009). The possibility of intra-particle diffusion was explored by using the intra-particle diffusion model (Weber and Morris, 1963)

$$q_t = K_{id}t^{1/2} + C \tag{6}$$

where K_{id} is the intra-particle diffusion rate constant (mg/g $min^{1/2}$) and C (mg/g) is a constant. If the Weber-Morris plot of q_t versus $t^{1/2}$ satisfies the linear relationship, the sorption process is found to be controlled only by intra-particle diffusion. However, if the data exhibit multi-linear plots, then two or more steps influence the sorption process. Figure 8 shows the intra-particle diffusion plots for OII onto organo-clays. The plots show multi-linearity correlation, which indicates that two steps occur during the adsorption process. The first portion is a gradual adsorption stage, where diffusion of the solute molecules on the surface of the adsorbents can be rate-controlling. The second stage is the final equilibrium. The correlation coefficients of the intra-particle diffusion model (Table II) are all high (>0.850), and they are significantly lower than for the pseudo-second-order kinetic

Table II. Intra-particular diffusion parameters for removal of Orange II by B-NHTPB and B-MTPB at different concentrations (V = 250 mL; m = 250 mg; pH = 6.5)

Adsorbents	C_0 (mg/L)	K_{id} (mg /g min$^{0.5}$)	C (mg/g)	R^2
B-N HTPB	50	1.1447	31.50	0.951
	100	1.6885	31.81	0.964
	150	1.3585	38.96	0.960
B-MTPB	50	0.2423	18.09	0.9339
	100	0.4520	21.3	0.9430
	150	0.2618	31.33	0.9369

model. The linear portion ended with a smooth curve followed by a linear portion. The two phases in the intra-particle diffusion plot suggest that the sorption process proceeds by surface sorption and intra-particle diffusion. Table II shows that the adsorption rate constant (K_{id}) onto B-NHTPB was far larger than that onto B-MTPB. Thus, the diffusion of OII was expected to be faster onto B-NHTPB than that onto B-MTPB. The difference in diffusion processes of Orange II onto B-NHTPB and B-MTPB is probably due to the greater extent of hydrophobicity exhibited by B-NHTPB in comparison with B-MTPB, due to the largest hexyl chain compared to methyl, thus making easier for OII to diffuse to the surface of the material or to penetrate through the inter-lamellar space.

The Effect of Temperature on Contact Time

The effect of temperature on the adsorption kinetics of OII by B-NHTPB and B-MTPB is studied at three temperatures (20, 40, and 60°C) with a constant initial dye concentration of 150 mg/L as shown in Figure 9. The adsorption capacity of the two materials is found to decrease with increasing temperature, i.e., 53.00 to 39.05 mg g^{-1} for B-NHTPB, and 33.51 to 16.16 mg g^{-1} for B-MTPB, respectively, when temperature increased from 20°C to 60°C. This indicates that the adsorption was favored at lower temperatures and controlled by an exothermic process. This may be due to a weakening of the attractive forces between OII and the adsorbents (Langmuir, 1916). The pseudo-first-order and pseudo-second-order models are used to evaluate the sorption kinetics at different temperatures, and the kinetic parameters
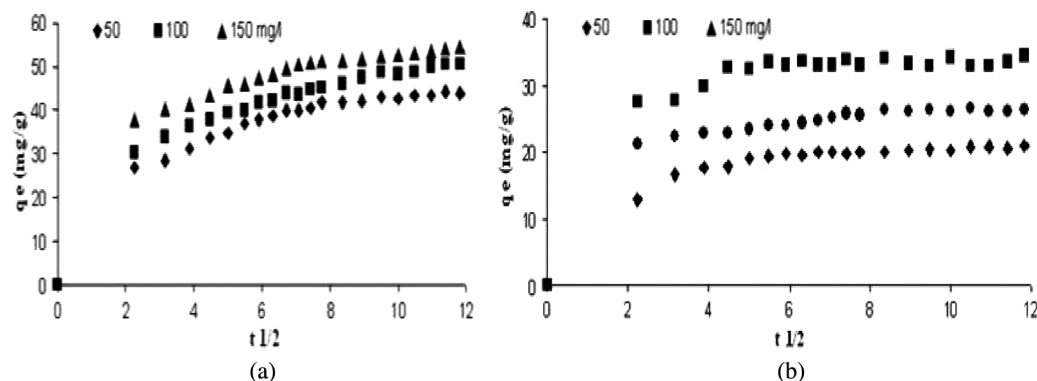

Fig. 8. Diffusion modelling of Orange II adsorption onto (a) B-NHTPB and (b) B-MTPB at various concentrations, pH 6.5, m/V = 1 g/L, T = 20°C.
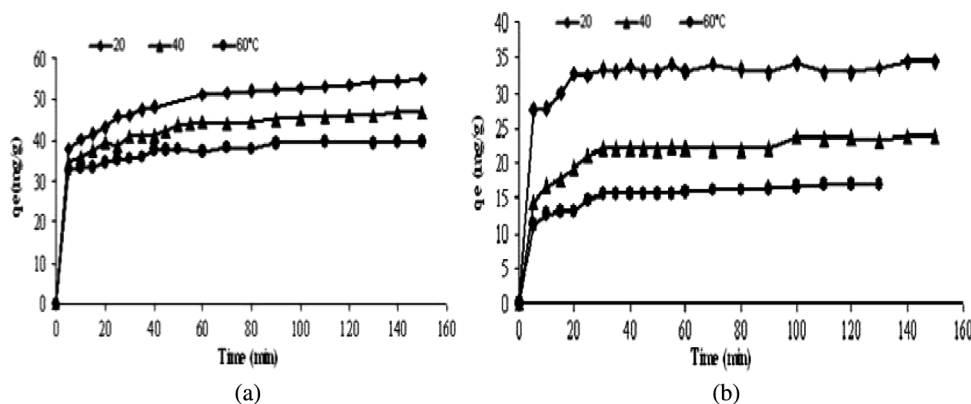
Fig. 9. Effect of temperature on the kinetics of Orange II by (a) B-NHTPB and (b) B-MTPB (m/V = 1 g/L, pH = 6.5, C_0 = 150 mg/L).

are shown in Table III, showing that the second-order kinetics is the best fit model for the adsorption of Orange II onto both adsorbents, as the correlation coefficient R_2^2 is higher than R_1^2.

The thermodynamic parameters of the adsorption process are determined from the experimental data obtained at different temperatures. The rate constant of the adsorption process is related to the temperature by means of the Arrhenius equation:

$$\ln K_2 = \ln A - \frac{E_a}{RT} \qquad (7)$$

In the present case, K_2 is the pseudo-second-order rate constant (g/mg/min), E_a is the Arrhenius activation energy of adsorption, A is the Arrhenius factor, R is the gas constant, and T is the temperature. The slope of the plot of lnK_2 versus $\frac{1}{T}$ (Figure 10) is used to evaluate E_a obtaining values of 17.91 and 13.45 kJ mol^{-1} for B-NHTPB and B-MTPB, respectively. Low activation energies (5–50 kJ mol^{-1}) are characteristics for physisorption, while higher activation energies (60–800 kJ mol^{-1}) suggest chemisorption (Deniz and Saygideger, 2010). So the results obtained here indicate that physisorption predominates in the present systems.

Adsorption Isotherms

The adsorption isotherms of Orange II onto the organoclays are shown in Figure 11. According to the classification of Giles et al. (1960), based on the initial slope and shape of

the upper part of curve, the adsorption isotherms are of L shape, subgroup 2 (Langmuir mono-layer). Adsorption isotherms describe how adsorbates interact with adsorbents and are crucial in optimizing the use of adsorbents.

The adsorption of OII onto the organo-clays was recorded in the concentration range from 30–200 mg/L, a fixed pH of 6.5, and temperatures of 20, 40, and 60°C. Figure 11 confirms that the adsorption decreases with the increase in temperature. It is also observed that the initial removal of dye is fast and the percentage uptake gradually decreases with the concentration. Similar results were reported in the adsorption of Orange II onto highly porous titania aerogel (Abramian and El-Rassy, 2009).

Langmuir (1918), Freundlich (1906), and Redlich-Peterson (1959) models have been considered in the present study. The Langmuir model assumes that adsorption takes place at specific homogeneous sites on the surface of the adsorbent and when a site is occupied by an adsorbate molecule, no further adsorption can take place at this site. Langmuir's equation is expressed by Eq. (8) (Langmuir, 1918):

$$q_e = \frac{q_{\max}bC_e}{1 + bC_e} \qquad (8)$$

where q_{max} (mg g^{-1}) is the Langmuir constant related to the maximum monolayer adsorption, and b (L mg^{-1}) is a constant related to the free energy or net enthalpy of adsorption.

The essential features of the Langmuir isotherm model can be expressed in terms of the dimensionless constant R_L,

Table III. Kinetic parameters for adsorption of Orange II depending on the temperature and applying the pseudo-first-order and the pseudo-second-order models

| Model Adsorbent	T (°C)	q_{exp} (mg/g)	Pseudo-first-order kinetic model			Pseudo-second-order kinetic model		
			q_{cal} (mg/g)	K_1(min^{-1})	R^2	q_{cal} (mg/g)	K_2(g/mg/min)	R^2
B-NHTPB	20	53.00	20.89	0.0398	0.988	56.17	0.0032	0.999
	40	45.51	15.15	0.0375	0.944	47.84	0.0043	0.999
	60	39.05	7.15	0.0280	0.853	40.32	0.0078	0.999
B-MTPB	20	33.51	08.99	0.1150	0.789	34.36	0.0087	0.999
	40	22.71	07.17	0.0390	0.884	23.92	0.0108	0.998
	60	16.16	08.22	0.1543	0.789	16.85	0.017	0.998
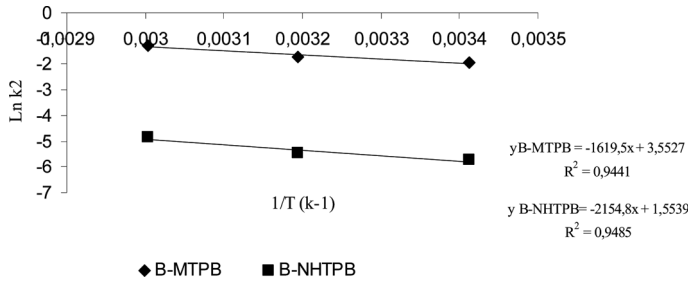
Fig. 10. The Arrhenius activation energy of adsorption.

separation factor, or equilibrium parameter, which is expressed by Eq. (9) (Hall et al., 1966):

$$R_L = \frac{1}{1 + bC_0} \qquad (9)$$

where b is the Langmuir constant (L/g) and C_0 is the highest initial dye concentration (mg/L). The R_L parameter is considered a more reliable indicator of the adsorption, and can adopt four values: for favorable adsorption $0 < R_L < 1$, for unfavorable adsorption $R_L > 1$, for linear adsorption $R_L = 1$, and for irreversible adsorption $R_L = 0$. The values of R_L calculated from the above equation are incorporated into Table IV. As the R_L values lie between 0 and 1, the on-going adsorption process is favorable.

The Freundlich model suggests a multilayer adsorption. Adsorption energy exponentially decreases on completion of the adsorption centers of an adsorbent. The Freundlich isotherm assumes that if the concentration of solute in the solution at equilibrium, C_e, is raised to the power n, the amount of solute adsorbed being q_e, then C_e^n is constant at a given temperature.

The Freundlich adsorption isotherm is expressed by Equation (10):

$$q_e = K_f C_e^n \qquad (10)$$

where K_f is adsorption capacity at unit concentration, and n is adsorption intensity; n values indicate the type of isotherm to be irreversible ($n = 0$), favorable ($0 \langle n \langle 1$), and unfavorable ($n \rangle 1$) (Alley, 2000).

The Redlich-Peterson isotherm model combines elements from both the Langmuir and Freundlich equations, where the mechanism of adsorption is a hybrid one and does not follow ideal monolayer adsorption. The Redlich-Peterson equation is widely used as a compromise between the Langmuir and Freundlich systems. It is expressed by Equation (11):

$$q_e = \frac{k_R C_e}{1 + \alpha_R C_e^\beta} \qquad (11)$$

k_R and α_R are the Redlich-Peterson isotherm constants and β is the exponent which lies between 0 and 1. The Redlich-Peterson isotherm incorporates three parameters and can be applied either in homogenous or heterogeneous systems.

The experimental data points fitted to the Langmuir, Freundlich, and Redlich-Peterson isotherm equations are shown in Figure 12. The characteristic parameters (q_{max}, b, k_f, n, k_R, $a_R\beta$) obtained in non-linear forms of Langmuir, Freundlich, and Redlich-Peterson (R-P) at several temperatures as well as the correlation coefficients R^2 are listed in Table IV.

The parameters obtained showed that the model which gives a good fit to the experimental data is the Langmuir model. The values of maximum adsorption capacity determined using the Langmuir expression are higher than the experimental adsorbed amounts and correspond to the adsorption isotherms plateaus. The maximum adsorption of Orange II based on the Langmuir isotherm is $53.78 \, \text{mg g}^{-1}$ for B-NHTPB and $33.79 \, \text{mg g}^{-1}$ for B-MTPB. The regression coefficients are higher from the Langmuir model, which suggests a best fitting of the Langmuir isotherm and that the adsorption occurs in the interlayer pores (Mittal et al., 2007).

The Redlich-Peterson isotherm was developed to improve the fitting between the Langmuir and the Freundlich equations. The value of parameter β shows whether the Langmuir isotherm ($\beta = 1$) or the Freundlich isotherm ($\beta = 0$) is preferable for the system. The value of 0.99 (close to 1) found for β indicates that the Langmuir isotherm is more appropriate.
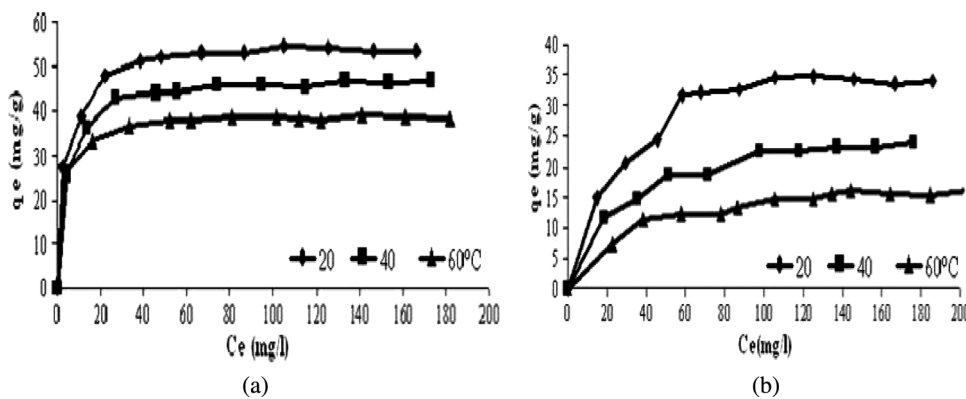

Fig. 11. Adsorption isotherms for Orange II onto (a) B-NHTPB and (b) B-MTPB at various temperatures.

Table IV. Freundlich, Langmuir, and Redlich-Peterson isotherm constants for the adsorption of Orange II by B-NHTPB and B-MTPB

Models		Langmuir					Freundlich			Redlich-Peterson			
	T(°C)	q_{exp} (mg/g)	q_{max} (mg/g)	b (L/g)	R_L	R^2	K_F (mg/g)	n	R^2	k_R (L/mg)	a_R (L/mg)	β	R^2
B-NHTPB	20	53.78	55.01	0.326	0.02	0.988	29.215	0.132	0.964	22.72	0.484	0.966	0.991
	40	46.20	47.66	0.269	0.02	0.997	25.76	0.185	0.969	13.41	0.291	0.992	0.997
	60	38.49	39.17	0.462	0.01	0.999	25.16	0.130	0.984	20.394	0.554	0.986	0.998
B-MTPB	20	33.79	41.71	0.041	0.13	0.973	9.164	0.26	0.931	1.007	4.27	1.331	0.986
	40	23.06	27.65	3.643	0.001	0.992	5.373	0.296	0.984	1.117	5.031	0.959	0.991
	60	15.29	18.55	0.032	0.17	0.983	3.645	0.287	0.971	0.593	3.159	1.002	0.984

(a)   (b)
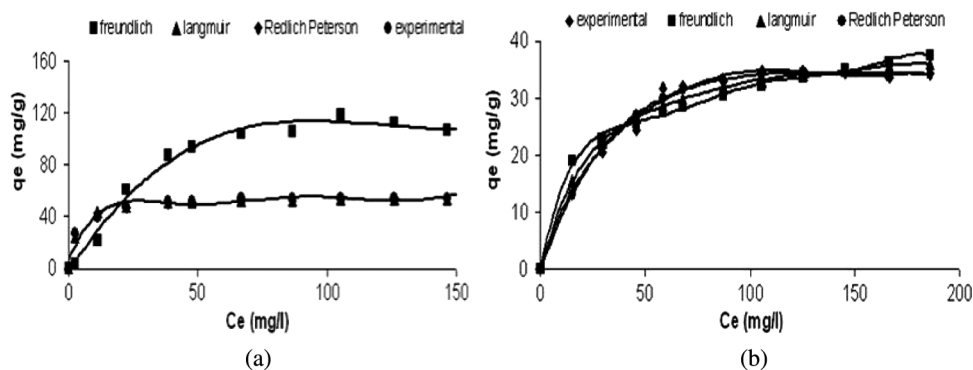
The Freundlich exponent n gives information about surface heterogeneity and surface affinity for the solute. The Freundlich exponent n between 0.130 and 0.296 indicates favorable adsorption. Since the degree of favorability increases as *n* approaches zero,

Table V shows the maximum adsorption capacity (q_e) for various adsorbents found in the literature. Several authors present this value in the experimental form or as the

maximum adsorption capacity of the monolayer obtained from the Langmuir isotherm.

Adsorption Thermodynamics

The spontaneity of a reaction is given by the well-known equation $\Delta G = \Delta H - T\Delta S$, where ΔG is the free energy change (kJ/mol), ΔH the adsorption enthalpy (kJ/mol),

Table V. Maximum adsorption capacity of the Orange II dyes by some adsorbents

| Adsorbants	qm (mg/g)	References
Sludge adsorbent (SA)	350.00	(Chiang et al., 2009)
Commercial activated carbon fibers	230.00	(Chiang et al., 2009)
Titania aerogel	420.00	(Abramian and El-Rassy, 2009)
HDTMA-montmorillonite	58.20	(Bae et al., 2000)
Cetylperidinium-montmorillonite	16.96	(Shin, 2008)
DMDOA-palygorskite	38.61	(Binoy et al., 2011)
Calcined hydrotalcite	1520	(Géraud et al., 2007)
Fly ash	82.80	(Janos et al., 2003)
Bottom ash	13.24	(Gupta et al., 2006)
Chitosan	116	(Uzun and Güzel, 2005)
Modified peat resin	71.43	(Sun and Yang, 2007)
Sludge from biological waste water plant	350	(Chiang et al., 2009)
De-oiled soya	9.58	(Gupta et al., 2006)
N-HTPB-montmorillonite	53.00	this study
MTPB-montmorillonite	33.51	this study
activated carbon	84.3	(Araceli et al. 2009)
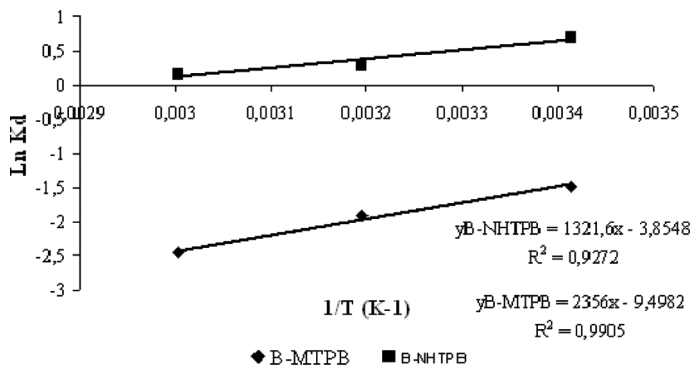
Fig. 13. Determination of standard enthalpy change for the adsorption of Orange II by B-NHTPB and B-MTPB.

Table VI. Thermodynamic parameters for the adsorption of Orange II by B-NHTPB and B-MTPB

Organo clay	T (°C)	$\Delta G°$ (kJ mol^{-1})	$\Delta H°$ (kJ mol^{-1})	$\Delta S°$ (J mol^{-1} K^{-1})
B-NHTPB	20	−1.59	−10.98	−32.03
	40	−0.95		
	60	−0.31		
B-MTPB	20	3.54	−19.58	−78.96
	40	5.12		
	60	6.70		

and ΔS the entropy change (J mol^{-1} K^{-1}). In the present case, the values of ΔH and ΔS are given by:

$$\ln K_d = \frac{\Delta S}{R} - \frac{\Delta H}{RT} \qquad (12)$$

$$K_d = \frac{q_e}{C_e} \qquad (13)$$

K_d being the Langmuir constant.

The values of ΔH and ΔS were obtained from the slope and intercept of the linear plot of lnK_d versus $\frac{1}{T}$ (Figure 13), and are given in Table VI. In the case of B-NHTPB, ΔG is negative, indicating that the process is spontaneous. However, in the case of B-MTPB positive ΔG values were observed at all three temperatures, indicating that spontaneity is not favored at this temperature (Hameed et al., 2009). In all cases, the adsorption happens as an exothermal process and with a decrease of the entropy of the systems.

Conclusion

In this study, two phosphonium organo-montmorillonites were selected as adsorbents for the removal of Orange II from aqueous solutions. FTIR and XRD data gave evidence on the intercalation of the alkyl-phosphonium cations onto the montmorillonite interlayer. Measurements of the d-spacing of the (001) peak increase in basal spacing was due to the introduction of phosphonium products in the bentonite

interlayer; the intercalation with NHTPB was more important than that with MTPB. The IR spectroscopic analysis of the unmodified clay (B-Na) and the modified clay B-NHTPB and B-MTPB revealed that the incorporation of the phenyl ring attached to the phosphonium atom displayed an unusually sharp and relatively strong vibration band at 1435 cm^{-1} in the clay galleries of B-Na during ion exchange reaction. Analysis of the kinetic and rate data, at different conditions (temperature and concentrations) using the pseudo-first-order, pseudo-second-order, and intra-particle diffusion models revealed that the pseudo-second-order sorption mechanism is predominant and the correlation coefficients are higher than 0.998.

The Langmuir model showed a better fit to adsorption data than the Freundlich one, the maximum capacity at 20°C and pH 6.5 was 53.78 and 33.79 mg/g for B-NHTPB and B-MTPB, respectively, The R_L values showed that B-NHTPB and B-MTPB were favorable for the adsorption of Orange II. Values of enthalpy change ($\Delta H°$) and entropy change ($\Delta S°$) were found at about −10.98 (kJ mol^{-1}) and −32.03 (J mol^{-1} K^{-1}), respectively, for the B-NHTPB and −19.58 (kJ mol^{-1}) and(−78.96 J mol^{-1} K^{-1}), respectively, for the B-MTPB.

The small positive value of the activation energy indicated low potential barriers and confirmed the physical mechanism of Orange II adsorption. The adsorption was exothermic and happened with a decrease of the entropy of the systems, the process being spontaneous for one of the adsorbents and non-spontaneous for the other.

Funding

References

Abramian, L., and El-Rassy, H. (2009). Adsorption kinetics and thermodynamics of azo-dye Orange II onto highly porous titania aerogel, *Chem. Eng. J.*, **150**, 403–410.

Alley, E. R. (2000). *Water Quality Control Handbook*, McGraw Hill, New York, N.Y., p. 125.

Araceli, R., Juan, G., Gabriel, O., and María, M. (2009). Adsorption of anionic and cationic dyes on activated carbon from aqueous solutions: Equilibrium and kinetics, *J. Hazard. Mater.*, **172**, 1311–1320.

Assaad, E., Azzouz, A., Nistor, D., Ursu, A.-V., Sajin, T., Miron, D., Monette, F., Niquette, P., and Hausler, R. (2007). Metals removal through synergic coagulation-flocculation using an optimized chitosan-montmorillonite system, *Appl. Clay Sci.*, **37**, 258–274.

Avalos, F., Ortiz, J. C., Zitzumbo, R., López-Manchado, M., Verdejo, A., and Arroyo, M. (2008). Effect of montmorillonite intercalant structure on the cure parameters of natural rubber, *J. Eur. Polym. J.*, **44**, 3108–3115.

Aydin, A. H., Sahin, E., and Akçay, G. (2004). The removal of dyes from water by modified bentonite, *Fres, Environ. Bull.*, **13**, 1530–1535.

Bae, J. A. E., Song, D., and Jeon, Y. (2000). Adsorption of anionic dye and surfactant from water onto organo-montmorillonite, *Sep. Sci. Technol.*, **35**, 353.

Bandara, J., and Kiwi, J. (1999). Fast kinetic spectroscopy, decolouration and production of H_2O_2 induced by visible light in oxygenated solutions of the azo dye Orange II, *New J. Chem.*, **23**, 717–724.

Baskaralingam, P., Pulikesi, M., Elango, D., Ramamurthi, V., and Sivanesan, S. (2006). Adsorption of acid dye onto organo-bentonite, *J. Hazard. Mater.*, **313**, 138–144.

Besson, G., Drits, V. A., Daynayak, L. G., and Smoliar, B. B. (1987). Analysis of cationic distribution in dioctahedral micaceous minerals of the basis IR spectroscopy data, *Clay Miner.*, **22**, 465–478.

Binoy, S., Yunfei, X., Mallavarapu, M., and Ravi, N, (2011). Orange II adsorption on palygorskites modified with alkyl trimethylammonium and dialkyl dimethylammonium bromide. An isothermal and kinetic study, *Appl. Clay Sci.*, **51**, 370–374.

Bouberka, Z., Kacha, S., Kameche, M., Elmaleh S., and Derriche, Z. (2005). Sorption study of an acid dye from aqueous solutions using modified clays, *J. Hazard. Mater.*, **119**, 117–124.

Chen, L., Deng, C, Wu, F., and Deng, N. (2011). Decolourization of the azo dye Orange II in a montmorillonite/H_2O_2 system, *Desalination*, **281**, 306–311.

Chiang, H.-M., Chen, T.-C., Pan, S. D., and Chiang, H. L. (2009). Adsorption characteristics of Orange II and chrysophenine on sludge adsorbent and activated carbon fibers, *J. Hazard. Mater.*, **161**, 1384–1390.

Chiu, Y. C., Huang, L. N., Uang, C. M., and Huang, J. F. (1990). Determination of the cation exchange capacity of clay minerals by potentiometric titration using divalent cation electrodes, *J. Colloid Surf.*, **46**, 327–337.

Deniz F., and Saygideger, S. D. (2010). Equilibrium, kinetic and thermodynamic studies of Acid Orange 52 dye biosorption by Paulownia tomentosa Steud. leaf powder as a low-cost natural biosorbent, Bioresour, *Technol.*, **101**, 5137–5143.

Freundlich, H. M. F. (1906). Uber die adsorption in lösungen, *Z. Phys. Chem.*, **57**, 385–470.

Géraud, E., Bouhent, M., Derriche, Z., Leroux, F., Prévot, V., and Forano, C. (2007). Texture effect of layered double hydroxides on chemisorption of Orange II, *J. Phys. Chem. Solids*, **68**, 818–823.

Giles, C. H., Mac Ewan, T. H., Nakhwa, S. N., and Smith, D. (1960). Studies in adsorption: Part XI. A system of classification of solution adsorption isotherms and its use in diagnosis of adsorption mechanisms and in measurement of specific surface areas of solids, *J. Chem. Soc.*, **III**, 3973–3993.

Gupta, V. K., Mittal, A., Gajbe, V., and Mittal, J. (2006). Removal and recovery of the hazardous azo dye Acid Orange 7 through adsorption over waste materials: Bottom ash and de-oiled soya, *J. Ind. Eng. Chem. Res.*, **4145**, 1446–1453.

Hall, K. R., Eagleton, L. C., Acrivos, A., and Vermeulen, T. (1966). Pore and solid-diffusion kinetics in fixed-bed adsorption under constant-pattern conditions, *Ind. Eng. Chem. Fundam.*, **5**, 212–223.

Hameed, B. H. (2009). Evaluation of papaya seeds as a novel non-conventional low-cost adsorbent for removal of methylene blue, *J. Hazard. Mater.*, **162**, 939–944.

Hameed, B. H., Ahmad, A. A., and Aziz N. (2009). Adsorption of reactive dye on palm-oil industry waste: Equilibrium, kinetic and thermodynamic studies, *Desalination*, **247**, 551–560.

Hang Pham, T., and Brindley G. W. (1970). Methylene Blue absorption by clay minerals. determination of surface areas and cation exchange capacities, (*Clay-Organic Studies* XVIII), *Clays Clay Miner.*, **18**, 203–212.

Hedley, C. B., Yuan, G. B., and Theng, K. G. (2007). Thermal analysis of montmorillonites modified with quaternary phosphonium and ammonium surfactants, *Appl. Clay Sci.*, **35**, 180–188.

Ho, Y. S., and McKay, G. (1998). Kinetic models for the sorption of dye from aqueous solution by wood, *Process Saf. Environ. Prot.*, **76**, 183–191.

Ho, Y. S., and McKay, G. (1999). Comparative sorption kinetic studies of dye and aromatic compounds onto fly ash, *J. Environ. Sci. Health A*, **34**, 1179–1204.

Ho, Y. S., Wase, D. A. J., and Forster, C. F. (1994). The adsorption of divalent copper ions from aqueous solution by sphagnum moss peat, *Trans. I. Chem. E, Part B: Proc. Safety Environ. Prot.*, **17**, 185–194.

Ijagbemi, C. O., Baek, M. H., and Kim, D. S. (2009). Montmorillonite surface properties and sorption characteristics for heavy metal removal from aqueous solutions, *J. Hazard. Mater.*, **166**, 538–546.

Janos, P., Buchtová, H., and Rýznarová, M. (2003). Sorption of dyes from aqueous solutions onto fly ash, *Water Res.*, **37**, 4938–4944.

Khalaf, H., Bouras, O., and Perrichon, V. (1997). Synthesis and characterization of Al-pillared and cationic surfactant modified Al-pillared Algerian bentonite, *Microp. Mater.*, **8**, 141.

Khenifi, A., Bouberka, Z., Bentaleb, K., Hamani, H., and Derriche, Z. (2009). Removal of 2,4-DCP from wastewater by CTAB/bentonite using one-step and two-step methods: A comparative study, *Chem. Eng. J.*, **146**, 345–354.

Khenifi, A. Bouberka, Z., Sekrane, F., Kameche, M., and Derriche, Z. (2007). Adsorption study of an industrial dye by an organic clay, *Adsorption*, **13**, 149–158.

Lagaly, G. (2006). Colloid Clay Science. In *Handbook of Clay Science-I. Developments in Clay Science*, eds. F. Bergaya, B. K. G. Theng, and G. Lagaly Elsevier, Amsterdam, pp. 87–113.

Lakshmi, U. R., Srivastava, V. C., Mall, I. D., and Lataye, D. H. (2009). Rice husk ash as an effective adsorbent: Evaluation of adsorptive characteristics for Indigo Carmine dye, *J. Environ. Manage.*, **90**, 710–720.

Langmuir, I. (1916). The constitution and fundamental properties of solids and liquids, Part I: Solids, *J. Am. Chem. Soc.*, **38**, 2221–2295.

Langmuir, I. (1918). The constitution and fundamental properties of solids and liquids, *J. Am. Chem. Soc.*, **40**, 1361–1403.

Lee, J. Y., and Lee, H. K. (2004). Characterization of organo-bentonite used for polymer nanocomposites, *Mat. Chem. Phys.*, **85**, 410–415.

Lee, S. H., Song, D. I., and Jeon, Y. W. (2001). An investigation of the adsorption of organic dyes onto organo-montmorillonite, *Environ. Technol.*, **22**, 247–254.

Madejova, J. (2003). FTIR techniques in clay mineral studies, *Vib. Spect.*, **31**, 1–10.

Makhoukhi, B., Didi, M. A., and Villemin, D. (2008). Modification of bentonite with diphosphonium salts: Synthesis and characterization, *Mat. Lett.*, **62**, 2493–2496.

Mittal, A., Kurup, L., and Mittal, J. (2007). Freundlich and Langmuir adsorption isotherms and kinetics for the removal of tartrazine from aqueous solutions using hen feathers, *J. Hazard. Mater.*, **146**, 243–248.

Mohamed, R., Lasheen, N. S., Ammar, H., and Ibrahim, S. (2012). Adsorption/desorption of Cd(II), Cu(II) and Pb(II) using chemically modified orange peel: Equilibrium and kinetic studies, *J. Solid State Chem.*, **14**, 202–210.

Nandi, B. K., Goswami, A., and Purkait, M. K. (2009). Adsorption characteristics of Brilliant Green dye on kaolin, *J. Hazard. Mater.*, **161**, 387–395.

Özcan, A. S., Erdem, B., and Özcan, A. (2004). Adsorption of Acid Blue 193 from aqueous solutions onto Na-bentonite and DTMA-bentonite, *J. Colloid Interface Sci.*, **280**, 44–54.

Patel, A. H., Somani, S. R., Bajaj, C. H., and Jasra, V. R. (2007). Preparation and characterization of phosphonium-montmorillonite with enhanced thermal stability, *Appl. Clay Sci.*, **35**, 194–200.

Permien, T., and Lagaly, G. (1995). The rheological and colloidal properties of bentonite dispersions in the presence of organic compounds-V. Bentonite and sodium montmorillonite and surfactants, *Clays Clay Miner.*, **43**, 229–236.

Qian, L., Yue, Q.-Y., Yuan, S., Gao, B.-Y., and Sun, H. J. (2010). Equilibrium, thermodynamics and process design to minimize adsorbent amount for the adsorption of acid dyes onto cationic polymer-loaded bentonite, *Chem. Eng. J.*, **158**, 489–497.

Redlich, O., and Peterson, D. L. (1959). A useful adsorption isotherm, *J. Phys. Chem.*, **63**, 1024–1029.

Ren, J. M., Wu, S. W., and Wei, J. (2010). Adsorption of Crystal Violet onto BTEA- and CTMA-bentonite from aqueous solutions, *Eng. Tech.*, **65**, 790–795.

Roberto, L. R., Araceli, J. A., Oliva, L., Torres, R, Rosa, M., Guerrero, C., Maria, S., Berber, M., and Pedro, A. D. (2008). Adsorption of chromium (vi) from water solution onto organobentonite, *J. Environ. Eng. Manage.*, **18**, 311–317.

Santhy, K., and Selvapathy, P, (2006). Removal of reactive dyes from wastewater by adsorption on coir pith activated carbon, *Bioresour. Technol.*, **97**, 1329–1336.

Schoonheydt, R. A., and Johnston, C. T. (2006). Surface and Interface Chemistry of Clay Minerals. In *Handbook of Clay Science*, eds. F. Bergaya, B. K. G. Theng, and G. Lagaly Elsevier, Amsterdam, pp. 87–113.

Shawabkeh, R. A., Al-Khashman, O. A., Al-Omari, H. S., and Shawabkeh, A. F. (2007). Cobalt and zinc removal from aqueous solution by chemically treated bentonite, *Environmentalist*, **27**, 357–363.

Shin, W. S. (2008). Competitive sorption of anionic and cationic dyes onto cetylpyridinium-modified montmorillonite, *J. Environ. Sci. Health. Part A: Toxic/Hazard. Sub. Environ. Eng.*, **43**, 1459–1470.

Sílvia, S. C. R., and Rui Boaventura, A. R. (2008). Adsorption modelling of textile dyes by sepiolite, *Appl. Clay Sci.*, **42**, 137–145.

Somasekhara, M. C., Reddy, L., Sivaramakrishna, A., and Varada, R. (2012). The use of an agricultural waste material, Jujuba seeds, for the removal of anionic dye (Congo red) from aqueous medium, *J. Hazard. Mater.*, **203–204**, 118–127.

Sun, Q. Y., and Yang, L. Z. (2007). Adsorption of acid orange II from aqueous solution onto modified peat-resin particles, *Huan Jing Ke Xue*, **28**, 1300–1304.

Sureshkumar, M. V., and Namasivayam, C. (2008). Adsorption behavior of Direct Red 12B and Rhodamine B from water onto surfactant-modified coconut coir pith, *Colloids Surf., A*, **317**, 277–283.

Uzun, I., and Güzel, F. (2005). Rate studies on the adsorption of some dyestuffs and p-nitrophenol by chitosan and monocarb oxymethyla ted(mcm)-chitosan from aqueous solution, *J. Hazard. Mater.*, **118**, 141–154.

Vadivelan, V., and Kumar, K. V. (2005). Equilibrium, kinetics, mechanism, and process design for the sorption of methylene blue onto rice husk, *J. Colloid Interface Sci.*, **286**, 90–100.

Vinka, A., James, O.-C., and Smith, A. (2006). Effect of quaternary ammonium cation loading and pH on heavy metal sorption to Ca bentonite and two organo-bentonites, *J. Hazard. Mater.*, **137**, 1102–1114.

Vogelpohl, A., and Kim, S. M. (2004). Advanced oxidation processes (AOPs) in wastewater treatment, *J. Ind. Eng. Chem.*, **10**, 33–40.

Walker, G. M., and Weatherley, L. R. (1999). Kinetics of acid dye adsorption on GAC, *Water Res.*, **33**, 1895–1899.

Weber, Jr., W. J., and Morris, J. C. (1963). Kinetics of adsorption on carbon from solution, *Eng. Div. Am. Soc. Civ. Eng.*, **89**, 31–59.

Xie, W., Xie, R., Pan, W.-P., Hunter, D., Koene, B., Tan, L.-S., and Vaia, R. (2002). Thermal stability of quaternary phosphonium modified montmorillonites, *Chem. Mater.*, **14**, 4837–4845.

Yilmaz, N., and Yapar, S. (2004). Adsorption properties of tetradecyl- and hexadecy trimethyl- ammonium-bentonites, *Appl. Clay Sci.*, **27**, 223.

Zaghouane-Boudiaf, H., and Boutahala, M. (2011). Adsorption of 2, 4, 5 trichlorophenol by organomontmorillonites from aqueous solutions: Kinetics and equilibrium studies, *Chem. Eng. J.*, **170**, 120–126.

Zhiyong, Yu., Mielczarski, E., Mielczarski, J., Laub, D., Buffat, Ph., Klehm, U., Albers, P., Lee Kulik, K. A., Kiwi-Minsker, L., Renken, A., and Kiwi, J. (2007). Preparation, stabilization and characterization of TiO2 on thin polyethylene films (LDPE). Photocatalytic applications, *Water Res.*, **41**, 862–874.

Zhu, L., and Ma, J. (2008). Simultaneous removal of acid dye and cationic surfactant from water by bentonite in one-step process, *Chem. Eng. J.*, **139**, 503–509.